J. Fluid Mech. (1986), vol. 169, pp. 257–274
Printed in Great Britain

The propagation of a Kelvin wave around a bend in a channel

By A. J. WEBB AND S. POND
Department of Oceanography, University of British Colombia,
6270 University Blvd., Vancouver, B.C. V6T 1W5, Canada

(Received 12 April 1985 and in revised form 10 February 1986)

The question is addressed of how much energy is reflected when a Kelvin wave propagating along a straight channel hits a bend. The solution is expressed as a truncated series of Kelvin waves and several evanescent cross-channel Poincaré modes. The bend acts as a diffraction grating – for bends of certain angles there is complete transmission and between these angles there are lobes of reflection. The width of the lobes of the diffraction pattern is directly proportional to the wavelength of the incident Kelvin wave, as in optics, electromagnetism, etc. The effect of changing the inside radius of the bend is also examined. The reflection of energy is generally small unless the Poincaré modes are nearly propagating.

1. Introduction

The problem of the reflection of a Kelvin wave from the end of a channel was first solved by Taylor (1920). He found that it was not possible for a pair of Kelvin waves propagating in opposite directions to satisfy the condition of zero flow normal to the endwall, and that a whole spectrum of Poincaré waves had to be involved in the reflection process. The problem was re-examined by Hendershott & Speranza (1971) and Brown (1973).

In this paper Taylor's method is used to investigate the behaviour of Kelvin wave incident upon a bend in a channel. This investigation was motivated by the question of how much of the internal tide in Knight Inlet, British Colombia is reflected by a right-angled bend half-way along. The internal tide is generated at a shallow sill, seaward of the bend, and propagates up-inlet until it hits the bend, where it is either reflected or transmitted and dissipated through turbulence. In an analysis of current-meter records, Freeland (1984) concluded that most of the internal tide is reflected by the bend. On the other hand, Blackford (1984), in a study of the waveform of the internal tide, deduced the opposite result. This study seeks to resolve the conflict between these two conclusions.

However, the results of this study are equally applicable to much wider channels, or to barotropic Kelvin waves; these factors are combined into a single parameter k, which is proportional to the ratio of the channel width to the incident wavelength.

Previous models of Kelvin waves propagating around bends have not included an opposite wall; they have been bends in straight coastlines. Buchwald (1968) considered a right-angled bend, and Packham & Williams (1968) solved the problem for a bend of general angle. Because there was no opposite wall, a reflected Kelvin wave was not possible, and any energy not transmitted as a Kelvin wave had to be radiated as cylindrical Poincaré waves from the corner. They found that there was complete transmission in the case of sub-inertial-frequency Kelvin waves, since the

Poincaré waves are evanescent. In the case of super-inertial-frequency Kelvin waves, Packham & Williams found that there was complete transmission only for wedge angles $\pi/(2n+1)$, where $n = 1, 2, 3, \ldots$ (see figure 10).

In this paper, then, solutions of the linearized long-wave equations in a flat-bottomed channel of rectangular cross-section are presented for the case of a Kelvin wave incident upon a bend. In §2 the governing equation and boundary conditions for the problem are presented, and in §3 the equations are non-dimensionalized and some special solutions (Kelvin and Poincaré waves) in a straight channel are given. Section 4 describes the method of solution in a bend in a channel, followed in §5 by a discussion of the eigenvalues for the problem in a sector of an annulus. The main results are presented in §6.

2. Governing equations

The linearized long-wave equations, for a harmonic time dependence $e^{i\omega t}$, separated into vertical and horizontal dependences, are (LeBlond & Mysak 1978, equations 10.34–10.38):

$$i\omega\tilde{U} - f\tilde{V} = -P_x, \tag{1}$$

$$i\omega\tilde{V} + f\tilde{U} = -P_y, \tag{2}$$

$$gh_n(\tilde{U}_x + \tilde{V}_y) = -i\omega P. \tag{3}$$

$(\tilde{U}, \tilde{V})$ and P are the horizontal dependences of velocity and pressure respectively, and h_n is the equivalent depth as derived from a vertical modes calculation. In the case of the barotropic tide, h_n is the depth of the channel.

Equations (1) and (2) can be solved for $\tilde{U}$ and $\tilde{V}$ in terms of P:

$$\tilde{U} = \frac{i\omega}{\omega^2 - f^2}\left(\frac{\partial}{\partial x} - i\tau\frac{\partial}{\partial y}\right)P, \tag{4}$$

$$\tilde{V} = \frac{i\omega}{\omega^2 - f^2}\left(\frac{\partial}{\partial y} + i\tau\frac{\partial}{\partial x}\right)P, \tag{5}$$

where

$$\tau \equiv f/\omega. \tag{6}$$

The equation of continuity (3) then yields the wave equation in P:

$$(\nabla^2 + \tilde{k}^2)P = 0, \tag{7}$$

where

$$\tilde{k}^2 \equiv (\omega^2 - f^2)/gh_n. \tag{8}$$

At a boundary, the requirement that there be no normal velocity is expressed by the condition:

$$\left(\frac{\partial}{\partial n} - i\tau\frac{\partial}{\partial s}\right)P = 0, \tag{9}$$

where n denotes the outward normal to the boundary, and s the direction along the boundary.

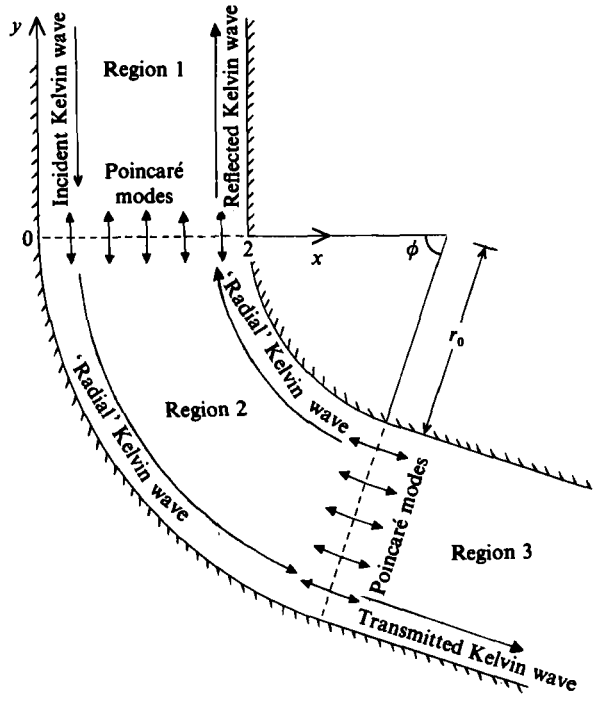

FIGURE 1. Schematic diagram of the annular bend, showing the geometry of the problem. The coordinate system used in describing solutions in a straight channel is shown in region 1.

3. Special solutions in a straight channel

The channel width is taken to be $2L$, and the lengthscale L is used to non-dimensionalize the space coordinates. The coordinate system shown in figure 1 is adopted, where the channel width is 2 units.

The problem then becomes

$$(\nabla^2 + k^2) P = 0, \tag{10}$$

with

$$\left(\frac{\partial}{\partial x} - \mathrm{i}\tau \frac{\partial}{\partial y}\right) P = 0 \quad \text{at } x = 0, 2, \tag{11}$$

where

$$k^2 \equiv \frac{\omega^2 - f^2}{g h_n} L^2. \tag{12}$$

Note that k^2 is a non-dimensional parameter.

The solution for a Kelvin wave propagating in the direction of increasing y is

$$P = \exp\left\{(\tau[x-1] - \mathrm{i}y) \frac{k}{(1-\tau^2)^{\frac{1}{2}}}\right\}, \tag{13}$$

$$U \equiv \left(\frac{\partial}{\partial x} - \mathrm{i}\tau \frac{\partial}{\partial y}\right) P = 0, \tag{14}$$

$$V \equiv \left(\frac{\partial}{\partial y} + \mathrm{i}\tau \frac{\partial}{\partial x}\right) P = \mathrm{i}k(1-\tau^2)^{\frac{1}{2}} P, \tag{15}$$

where U, V are proportional to the velocities $\tilde{U}$, $\tilde{V}$.

The corresponding expressions for the mth cross-channel Poincaré mode are

$$P = \mathrm{e}^{-k_m y}\left(\cos t_m x - \frac{\mathrm{i}\tau k_m}{t_m}\sin t_m x\right), \tag{16}$$

$$U = \mathrm{e}^{-k_m y}\left(\frac{\tau^2 k_m^2 - t_m^2}{t_m}\right)\sin t_m x, \tag{17}$$

$$V = \mathrm{e}^{-k_m y}\left((\tau^2 - 1)\, k_m \cos t_m x - \frac{\mathrm{i}\tau k^2}{t_m}\sin t_m x\right), \tag{18}$$

for $m = 1, 2, 3, \ldots$,

where
$$t_m \equiv \tfrac{1}{2}m\pi, \tag{19}$$

and
$$k_m \equiv +(t_m^2 - k^2)^{\frac{1}{2}}. \tag{20}$$

In this paper it is assumed that all the Poincaré modes are evanescent, i.e. $k^2 < (\frac{1}{2}\pi)^2 = 2.4674$, and that the frequencies are super-inertial, i.e. $\tau = (f/\omega) < 1$. Equations (12) and (20) show that all sub-inertial-frequency Poincaré waves (e.g. diurnal tides) are evanescent, whereas super-inertial-frequency Poincaré waves (e.g. semi-diurnal tides) will only propagate if the channel is wide enough or the phase speed $(gh_n)^{\frac{1}{2}}$ is small enough. Kelvin waves propagate at all frequencies.

The corresponding expressions for Kelvin waves propagating in the opposite direction can be obtained by replacing k by $-k$ in (13)–(15), or for Poincaré waves decaying in the opposite direction by replacing k_m by $-k_m$ in (16)–(18).

For reference, expressions for the non-dimensional wavelength of the incident Kelvin wave λ, and the non-dimensional Rossby radius R_0, are

$$\lambda = 2\pi\frac{(1-\tau^2)^{\frac{1}{2}}}{k}, \tag{21}$$

$$R_0 = \frac{(1-\tau^2)^{\frac{1}{2}}}{\tau k}. \tag{22}$$

The appropriate lengthscale to convert these to dimensional quantities is L, the half-width of the channel.

4. Method of solution

The domain of interest is a bend in a channel, as shown in figure 1. The domain is split into three regions – two straight channels (regions 1 and 3) and a sector of an annulus of variable angle (region 2). The two free parameters that describe the geometry of the bend are the bend angle ϕ and the inside radius of the bend r_0.

The solutions in regions 1 and 3 are expressed as a sum of a Kelvin wave propagating away from the boundary with region 2, and a truncated infinite series of evanescent Poincaré modes, which decay away from the same boundary. These waves all have unknown complex coefficients that must be determined. In addition, the solution in region 1 has a further component, namely an incident Kelvin wave of unit amplitude and zero phase.

The solution in region 2 is expressed as a superposition of 'radial' Kelvin waves and Poincaré modes. If the solution $P(r, \theta)$ is separated into

$$P(r, \theta) = R(r)\,\Theta(\theta) \tag{23}$$

then the wave equation becomes

$$\Theta'' = -\nu^2\Theta \tag{24}$$

and

$$R''+\frac{1}{r}R'+\left(\frac{-\nu^2}{r^2}+k^2\right)R = 0, \tag{25}$$

where ν^2 is the separation constant. The solution to the θ-problem is

$$\Theta = \mathrm{e}^{\mathrm{i}\nu\theta}. \tag{26}$$

The boundary conditions of zero normal flow at the inner and outer radii of the annulus become

$$U_r \equiv R'+\frac{\tau\nu}{r}R = 0 \quad \text{at} \quad r = r_0,\ r_0+2. \tag{27}$$

Equations (25) and (27) form an eigenvalue problem, whose eigen-functions form a complete set. The corresponding expression for the velocity component parallel to the channel is

$$V_\theta \equiv \frac{\mathrm{i}\nu}{r}R+\mathrm{i}\tau R'. \tag{28}$$

Equation (25) is Bessel's equation of order ν. For 'radial' Kelvin waves, the eigenvalue ν is real, and the solution could be expressed in terms of Bessel functions of order ν. However, for evanescent 'radial' Poincaré modes, ν is nearly imaginary (it is a complex number whose phase is close to 90° or 270°; see discussion in §5). The eigenvalue problem was solved numerically, since this method is easier than evaluating Bessel functions of complex order. A fourth-order Runge–Kutta scheme was used with iterative refinement of the eigenvalue to satisfy the boundary condition at the end point of the integration (a 'shooting' technique).

The solution in the annulus was expressed as a superposition of two 'radial' Kelvin waves propagating in opposite directions around the annulus, and the two corresponding truncated sets of Poincaré modes, decaying in opposite directions.

Hence, if the Poincaré modes are truncated after M terms, then $4(M+1)$ complex coefficients are required to describe the solution everywhere. All the basis functions satisfy the wave equation, and they satisfy the boundary condition of zero normal velocity along the coastline. However, the matching of pressure and velocity along the common boundaries between regions 1 and 2 and between 2 and 3 remain to be imposed.

In fact, it is only necessary for the pressure and normal velocity to be matched across these boundaries, since if these two properties match then all other properties, including tangential velocity, must also match. Suppose that the pressure matches on either side of a boundary. Then the tangential component of the pressure gradient $\partial P/\partial s$ must match. Yet if the normal velocity $(\partial P/\partial n - \mathrm{i}\tau\,\partial P/\partial s)$ matches then $\partial P/\partial n$ also matches. Hence ∇P matches, and so therefore does the tangential velocity $(\partial P/\partial s + \mathrm{i}\tau\,\partial P/\partial n)$. We also have $(\nabla^2+k^2)P = 0$ on both sides of the boundary, which implies that $(\nabla^2+k^2)\nabla P = 0$, $(\nabla^2+k^2)\nabla^2 P = 0$, etc. Given that P and ∇P match, it follows by induction that $\nabla^2 P$, $\nabla^3 P$, $\nabla^4 P$, etc., also match.

The matching process was split into two stages, which reduced the problem from the inversion of a complex matrix of order $4(M+1)$ to the inversion of two matrices of order $2(M+1)$.

4.1. *First stage*

The first stage is the matching of normal velocity. The problem of a basin of the form of a sector of an annulus with zero normal velocity along one straight edge and a prescribed normal velocity along the other is considered.

The solution inside the annulus can be expressed as a sum of two 'radial' Kelvin waves propagating in opposite directions, and their two associated sets of M 'radial' Poincaré modes, decaying in opposite directions. The solution requires $2(M+1)$ complex coefficients to be determined. The boundary conditions of zero normal velocity along one straight edge and prescribed normal velocity along the other must be forced by a suitable choice of coefficients.

The coefficients were calculated using a least-squares method, minimizing the sum of squares of the moduli of the differences between the normal velocities corresponding to the fitted superposition of basis functions and the required normal velocity. The sum of squares was calculated by dividing each boundary into $N-1$ intervals, and then evaluating the basis functions and required normal velocities at N points distributed evenly along each of the two boundaries. The value of N was chosen to be sufficiently large ($\geqslant 2M$) that aliasing of the Poincaré modes did not occur. Hence the $2(M+1)$ unknowns were calculated by a least sum of squares at $2N$ locations.

The first stage, then, consists of applying this procedure $2M+3$ times with the following prescribed normal velocities to region 2:

(*a*) the normal velocity corresponding to an incident Kelvin wave in region 1;
(*b*) the normal velocity corresponding to a reflected Kelvin wave in region 1;
(*c*) the normal velocity corresponding to each of M evanescent Poincaré modes in region 1;
(*d*) the normal velocity corresponding to a transmitted Kelvin wave in region 3;
(*e*) the normal velocity corresponding to each of M evanescent Poincaré modes in region 3.

At this stage the amplitude and phase of all these applied waves were arbitrarily set to unity and zero. Their actual magnitude and phase are determined in the second stage.

4.2. *Second stage*

The second stage is the matching of pressure. For each of the $2M+3$ types of wave in the straight channels, the first stage of the calculation returns the pressure field inside region 2 such that the normal velocity matches. For each of these waves, the difference between the pressure in region 2 and that in regions 1 and 3 is calculated along their two common boundaries. If the wave exists in region 1, then the pressure in region 3 is taken to be zero, and vice versa.

The aim of the second stage is to find a combination of the $2M+3$ types of wave in the straight channels that makes the sum of these 'pressure anomalies' vanish. The amplitude and phase of the incident Kelvin wave are arbitrarily set to unity and zero, leaving $2(M+1)$ complex coefficients to be calculated. They are also evaluated by a least-sum-of-squares method – minimizing the sum of squares of the moduli of the 'pressure anomalies' at $2N$ locations.

The first stage of the calculation describes how a sector of annulus responds to various forcing terms, and the second stage describes how the annulus and the two straight channels are connected. This method is an adaptation of the collocation method. However, in the collocation method boundary conditions are applied at the

same number of points as there are unknown coefficients. In this method at least twice as many points are used, and the boundary conditions are applied in a least-squares sense.

5. Discussion of the results of the eigenvalue problem in the annulus

The eigenvalues $\{\nu_i\}$ for the radial Kelvin and Poincaré modes were found to be of the same order of magnitude as those in a straight channel of the same width. A value must be assigned to the radius when converting from polar coordinates to Cartesian coordinates; this value was taken to be the average radius of the annulus (r_0+1). As the radius of the annulus tended to infinity, the eigenvalues ν_i tended to the eigenvalues in a straight channel, as expected.

The eigenvalues for Kelvin waves in a straight channel are real, and for evanescent Poincaré modes are imaginary. In both cases, the eigenvalues corresponding to waves propagating (or decaying) in the opposite direction are the negative of the original eigenvalues.

However, in a bend, when there is rotation, a 'splitting' occurs. As f is increased from zero, or as r_0 is decreased from infinity, the eigenvalue for a Kelvin wave propagating around a bend to the left increases slowly above its original value. The eigenvalue for a Kelvin wave propagating around a bend to the right decreases slowly below its original value. For sharp bends ($r_0 = 0.1$ say), this difference between the eigenvalues for bends of opposite senses is large. This effect can be explained in terms of the difference in path lengths for a Kelvin wave bound tightly to the right-hand side of the channel. Such a wave propagating around a bend to the right will have a larger angular velocity than a wave propagating around a bend to the left for a given linear phase speed because of the shorter path length. Hence its angular wavenumber will be smaller.

The eigenvalues for Kelvin waves do, however, remain real. The cross-channel pressure distribution also stays real, and the along-channel velocity component is still imaginary. However, a small, real cross-channel velocity component is introduced. This quantity is small at first, but increases as r_0 decreases.

The eigenvalues for the evanescent Poincaré modes are no longer imaginary, but a small real part is introduced as the sharpness of the bend is increased. It can be shown that the eigenvalue for a Poincaré mode decaying clockwise around a bend is the complex-conjugate of the eigenvalue for one decaying anticlockwise around a bend. This small real part to the eigenvalues is equivalent to a long-wavelength oscillation which is quickly damped out by the presence of the imaginary part. The real part always has a sign such that the oscillation propagates around the bend in an anticyclonic direction (clockwise in the northern hemisphere).

6. Main results

The following results were obtained using 10 Poincaré modes ($M = 10$), and doing a least-squares fit at 20 points along each boundary ($N = 20$). The success of each run was judged by the extent to which the pressure and velocity fields were continuous across the boundaries, and the extent to which the sum of the transmitted and reflected energy fluxes equalled the incident flux.

The continuity of velocity can be evaluated by looking at the plot of current ellipses – for points on the common boundary between two regions two ellipses are

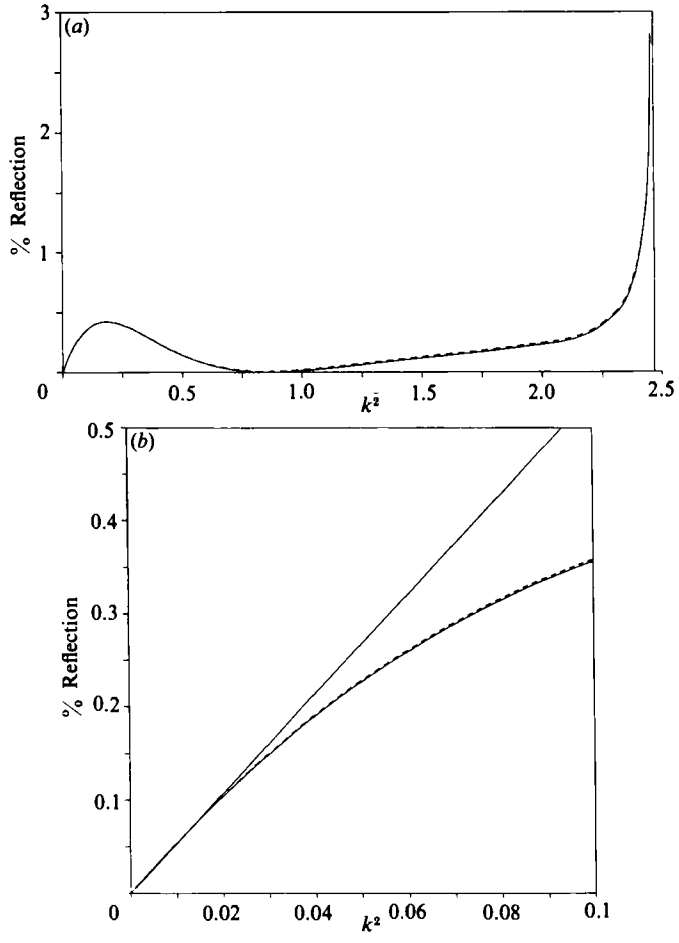

FIGURE 2. (*a*) Reflection coefficient against k^2: $\tau = 0.803$,, $r_0 = 0.5$, $\phi = 90°$. Solid line is $R\%$, dashed line is $100 - T\%$. The first Poincaré mode propagates when $k^2 > 2.4674$. (*b*) Blowup of (*a*) for small k^2. The straight line is $R\% = 5.34\ k^2$, which is the least-squares best fit for $k^2 < 0.025$.

plotted according to the solution in each region. The two ellipses should be indistinguishable. Note that the current ellipses in all the figures are scaled by an arbitrary factor to make the ellipses large enough to be seen clearly without excessive overlapping.

The relative energy fluxes were calculated by simply squaring the absolute value of the coefficient of the relevant wave in the solution, be it the incident, reflected or transmitted wave. The reflected ($R\%$) and transmitted ($T\%$) fluxes were expressed as a percentage of the incident flux. There should be no energy loss, since there is no dissipation in the model. The Poincaré modes transmit no energy, since they are evanescent.

There are four free parameters in the problem, namely τ, the period of the oscillation, k, which is proportional to the ratio of the channel width to the Rossby radius (the Burger number), ϕ, the bend angle, and r_0, the inside radius.

The approach used was to keep three of these parameters constant, and vary the fourth. The standard values used to start each parameter search were $\tau = 0.803$,

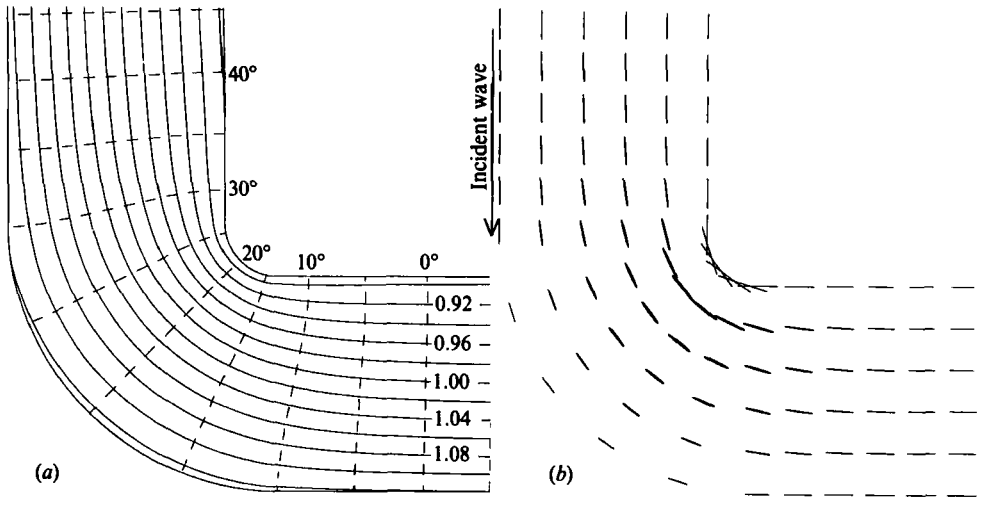

FIGURE 3. Solution fields for the case $k^2 = 7.02 \times 10^{-3}$, $\tau = 0.803$, $r_0 = 0.5$, $\phi = 90°$. Derived values: $\lambda = 44.7$, $R_0 = 8.8$, $R\% = 0.038\%$, $100 - T\% = 0.038\%$. (*a*) Pressure field: solid lines are contours of magnitude; dashed lines are contours of phase. (*b*) Velocity field: current ellipses are plotted.

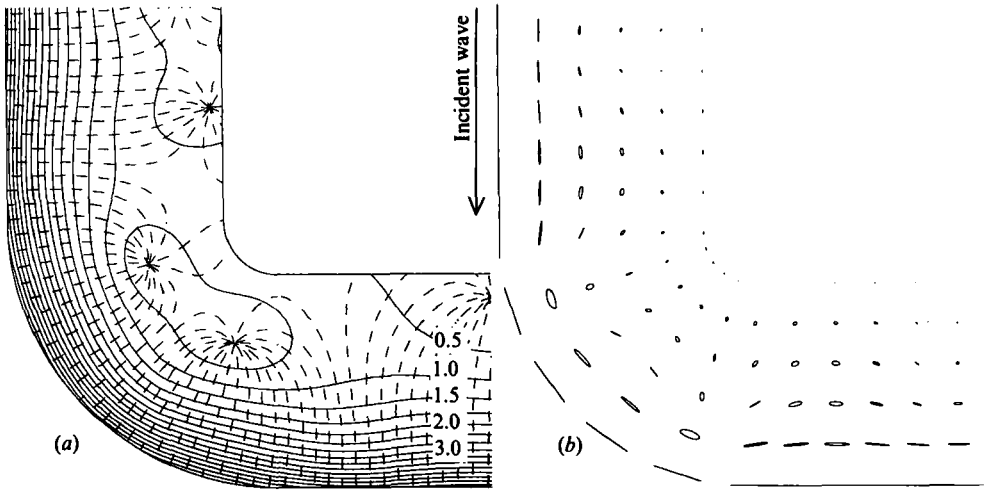

FIGURE 4. Solution fields for the case $k^2 = 2.25$, $\tau = 0.803$, $r_0 = 0.5$, $\phi = 90°$. Derived values: $\lambda = 2.5$, $R_0 = 0.49$, $R\% = 0.394\%$, $100 - T\% = 0.408\%$. (*a*) Pressure field. (*b*) Velocity field.

$k^2 = 7.02 \times 10^{-3}$, $\phi = +90°$ (a right-angled bend to the left), $r_0 = 0.5$. These were chosen to represent the first mode of the M2 constituent of the internal tide in Knight Inlet.

6.1. $\tau = 0.803$, $\phi = +90°$, $r_0 = 0.5$, *variable* k^2

Figure 2 shows plots of the reflection coefficient $R\%$ against k^2 for constant τ, r_0 and ϕ. $R\%$ is remarkably small ($< 1\%$) until just before the cutoff wavenumber at which Poincaré waves start to propagate, where there is a sharp rise. For small k^2 (< 0.05), $R\%$ is roughly linear in k^2, and the curve approaches the line $R\% = 5.34k^2$ as $k^2 \to 0$ (see blowup in figure 2*b*).

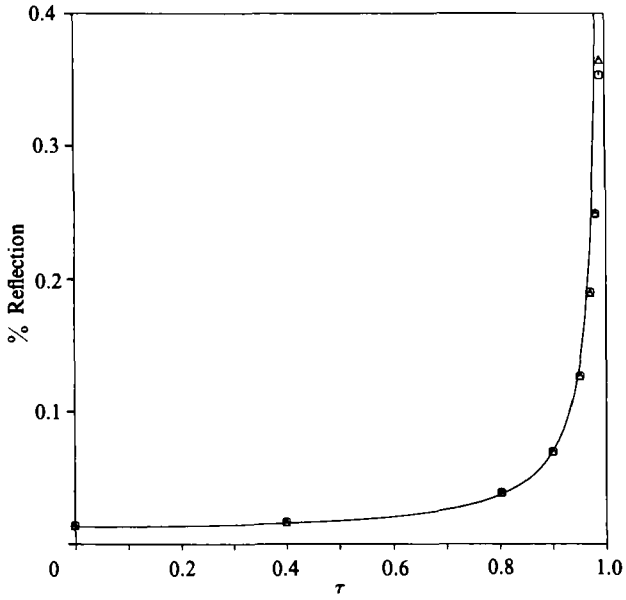

FIGURE 5. Reflection coefficient against τ: $k^2 = 7.02 \times 10^{-3}$, $r_0 = 0.5$, $\phi = 90°$. Triangles are $R\%$, circles are $100 - T\%$. Solid line is the curve $R\% = 1.89\, k^2/(1-\tau^2)$, which is the best fit to the points.

The standard values for Knight Inlet lie well within the linear part of the relationship. Figure 3 shows the pressure and velocity fields for these values of the parameters. Note that because of the assumed $e^{i\omega t}$ time dependency waves propagate in the direction of decreasing phase (Arg P). Figure 4 shows the pressure and velocity fields for $k^2 = 2.25$. This value lies in the rising portion of the curve of $R\%$ *vs.* k^2. Note the presence of amphidromes where the magnitude of the pressure oscillation is zero, and hence its phase is ambiguous. Derived values for the wavelength of the Kelvin wave λ and the Rossby radius R_0 are included in the captions of figures 3 and 4.

In all cases the current ellipses and pressure contours were observed to match very well, and no normal velocity component was observed at the boundaries. Agreement between $R\%$ and $100 - T\%$ was excellent.

6.2. $k^2 = 7.02 \times 10^{-3}$, $\phi = +90°$, $r_0 = 0.5$, *variable* τ

Figure 5 shows the effect of varying τ with a constant, small k^2 in a right-angled bend. A $1/(1-\tau^2)$ dependency was observed. Combining this relationship with the linear relationship obtained for small k^2 leads to the empirical relationship

$$R\% = 1.89 \frac{k^2}{1-\tau^2} \quad \text{for small } k^2. \tag{29}$$

Using (21) one sees that $R\%$ is directly proportional to the square of the ratio of the channel width to the wavelength of the incident Kelvin wave, for long waves.

The case of sub-inertial-frequency waves $\tau > 1$ was also attempted. Unfortunately the method of solution broke down, in the sense that the velocity matching could not be achieved, and energy was not conserved. It is necessary to use negative values for k^2 when $\tau > 1$, since $f > \omega$ (see (12)). The following possible causes of the breakdown were carefully investigated, without success:

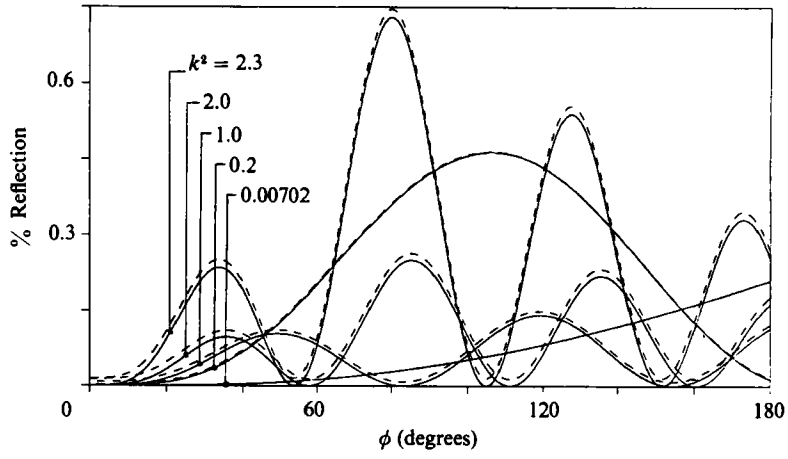

FIGURE 6. Reflection coefficient against bend angle ϕ for various values of k^2: $\tau = 0.803$, $r_0 = 0.5$. Solid lines are $R\%$, dashed lines are $100-T\%$.

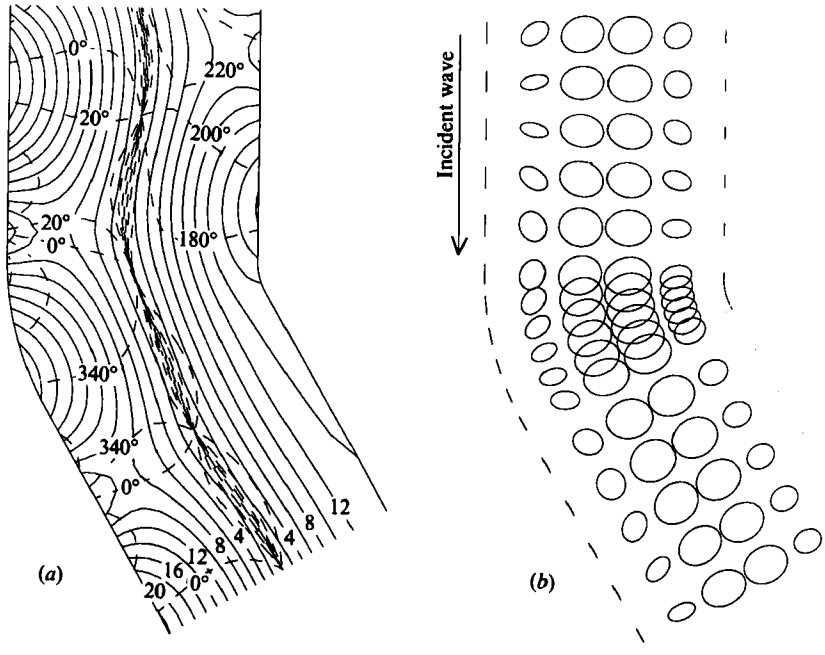

FIGURE 7. Solution fields for the case $k^2 = 2.467$, $\tau = 0.803$, $r_0 = 0.5$, $\phi = 30°$. Derived values: $\lambda = 2.4$, $R_0 = 0.47$, $R\% = 35.93\%$, $100-T\% = 36.00\%$. (*a*) Pressure field. (*b*) Velocity field. The curved line at the inside corner is a result of several short ellipses running into each other.

(*a*) ill-conditioning of the matrices;
(*b*) incorrect determination of the eigenfunctions in the annulus;
(*c*) resonance in the sector of the annulus, caused by using a pair of (k^2, τ)-values that would allow free modes in a closed sector of an annulus (this would result in singular matrices);
(*d*) programming error.

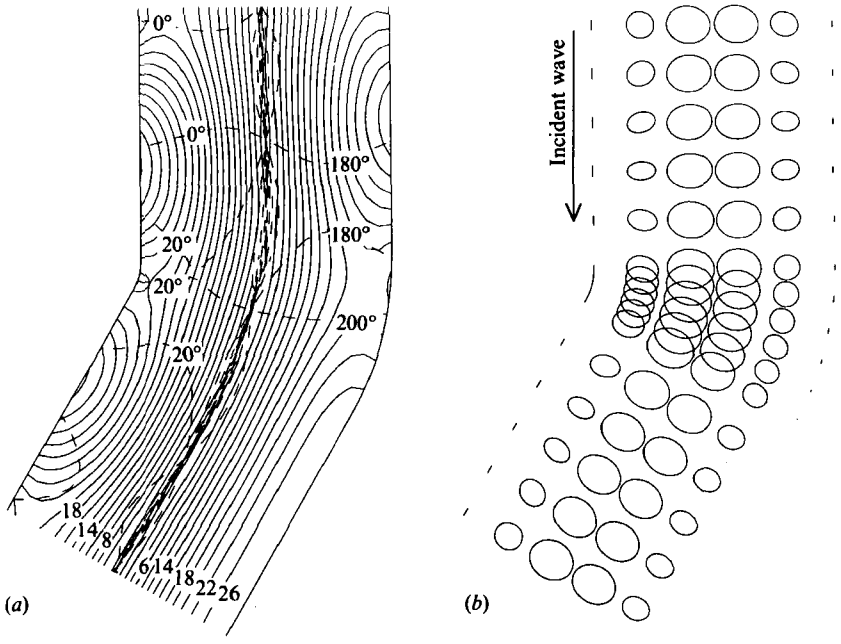

FIGURE 8. Same as figure 7 except $\phi = -30°$ (i.e. a bend to the left). Derived values: $R\% = 35.88\%$, $100 - T\% = 36.42\%$.

6.3. $\tau = 0.803$, $r_0 = 0.5$, *various* k^2, *variable* ϕ

Figure 6 shows the effect of varying the bend angle ϕ. Two observations can be made: there are certain angles for which there is zero reflection; and there is no significant difference in reflection coefficient for a bend of a given angle to the left and a bend of the same angle to the right (i.e. figure 6 is symmetrical about the $R\%$-axis $\phi = 0$). Results for negative ϕ are not actually plotted because they are the mirror image of results for positive ϕ.

The effect of increasing k^2 is to compress the peaks laterally (i.e. make the zeros closer together), and to make them higher. The case $k^2 = 2.467$ was also calculated, but was not included in figure 6 because it would have gone off scale. It can be seen in figure 9(*c*) on different axes.

Examination of figure 6 reveals why there is a minimum in figure 2(*a*) at around $k^2 = 0.75$. The first angle of zero reflection decreases as k^2 increases, and passes over the value $\phi = 90°$ at this value of k^2.

Figures 7 and 8 illustrate the pressure and velocity fields for bends of 30° to the left and right respectively; they both have the same reflection coefficient (36 %). The value used for k^2 is 2.467, which is just below the cutoff value at which the first Poincaré wave propagates. This value was chosen to give a large $R\%$. In fact, the e-folding length for the decay of the Poincaré mode is $50L$ (i.e. 25 times the channel width), and the solution is dominated by this mode. Its amplitude is an order of magnitude higher than that of the Kelvin waves. The dominance of the Poincaré mode is the reason for the characteristic change in phase of the pressure in mid-channel by 180°, and the maximum in velocities in mid-channel in figures 7 and 8 (see (16)–(18) with very small k_m). There is no along-channel phase propagation because the Poincaré mode is evanescent. The Poincaré mode does not contribute any energy flux, but it does dominate the solution near the bend, say within $100L$ of the bend.

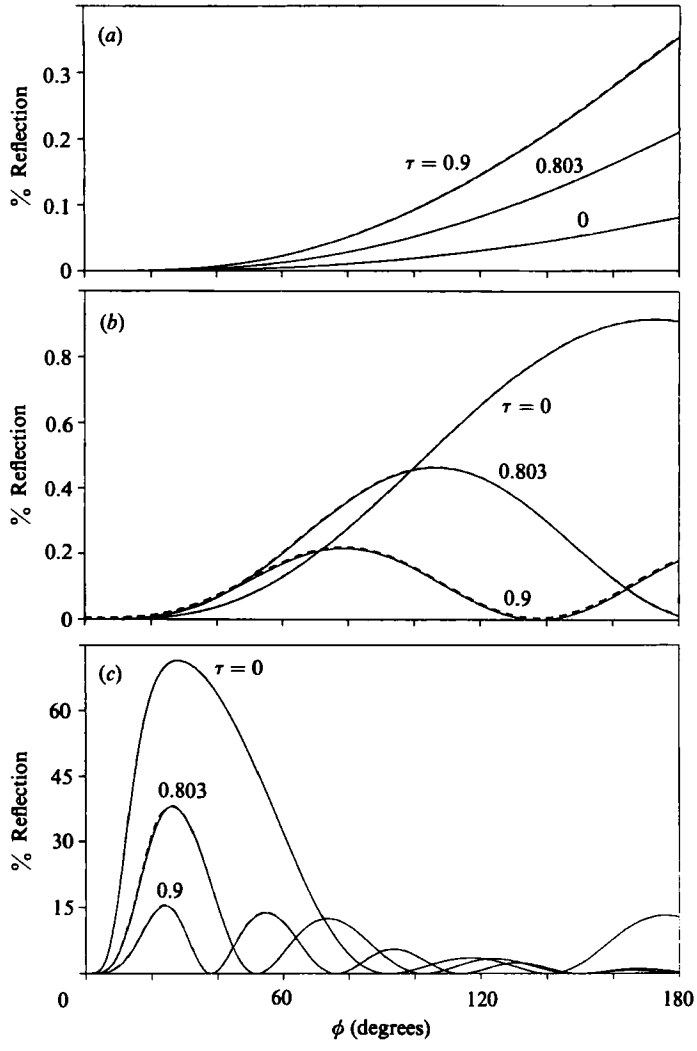

FIGURE 9. Reflection coefficient against bend angle ϕ for various values of τ. $r_0 = 0.5$. Solid lines are $R\%$, dashed lines are $100\text{–}T\%$. (*a*) $k^2 = 7.02 \times 10^{-3}$; (*b*) 0.2; (*c*) 2.467.

The generation of a large-amplitude Poincaré mode seems to be associated with the occurrence of high reflection coefficients for the Kelvin wave, and occurs when the Poincaré mode has a large decay scale (almost propagating). Brown (1973) found a similar result in his study of the reflection of a Kelvin wave from the end of a channel (the Taylor problem). He allowed the first Poincaré mode to propagate, so that any energy not reflected as a Kelvin wave was reflected as a Poincaré wave. He found that just above the critical frequency at which the first Poincaré mode starts to propagate (i.e. k^2 just above $(\frac{1}{2}\pi)^2$), this mode becomes the principal energy-reflection mechanism.

It therefore seems likely that soon after the first Poincaré mode starts to propagate it will rapidly become a dominant energy radiation mechanism in the bend too, although in which direction is open to speculation. The amplitude of the Poincaré mode has already been seen to become very large for k^2 just less than $(\frac{1}{2}\pi)^2$, although as long as the mode is evanescent it cannot contribute to the

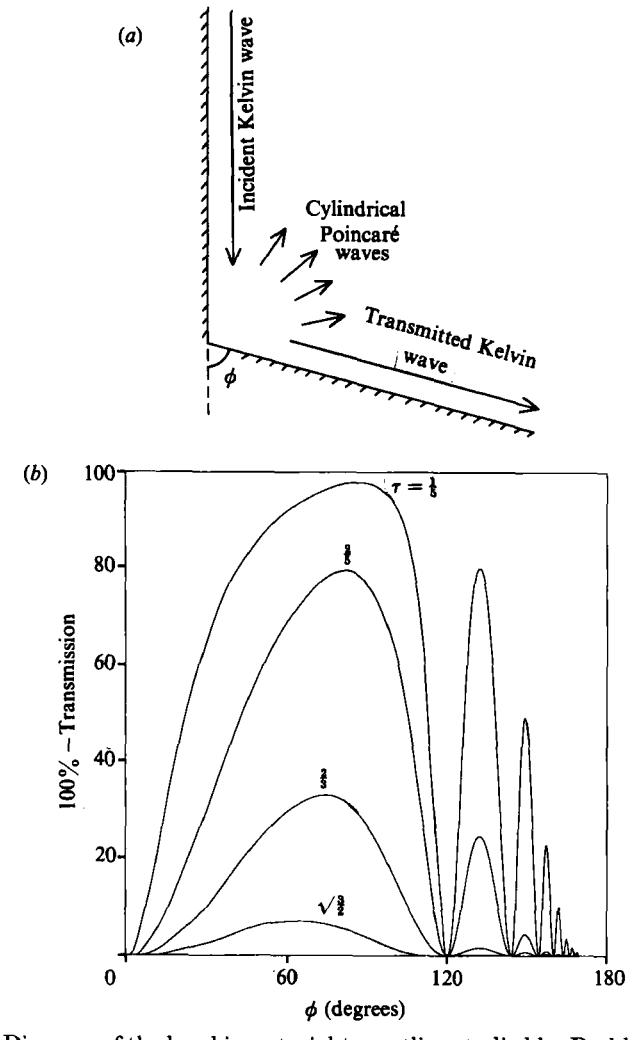

FIGURE 10. (*a*) Diagram of the bend in a straight coastline studied by Packham & Williams (1968). (*b*) $100-T\%$ against bend angle ϕ for various values of τ (after Packham & Williams 1968).

energy-flux budget. However, as k^2 increases above $(\frac{1}{2}\pi)^2$, it is only necessary for the magnitude of that mode to remain large for the energy flux to increase rapidly, since the group velocity C_g will increase rapidly anyway. Brown showed that if $k^2 = (\frac{1}{2}\pi)^2\,(1+\delta)$, then $C_g = O(\delta^{\frac{1}{2}})$.

6.4. $r_0 = 0.5$, *various* k^2, *various* τ, *variable* ϕ

Figure 9 shows plots of $R\%$ against bend angle ϕ for various values of k^2 and τ.

For small k^2 (figure 9*a*), larger values of τ lead to larger values of $R\%$ for all angles. The system is in the $1/(1-\tau^2)$ regime. However, for large k^2 (figure 9*c*), larger values of τ lead to smaller values of $R\%$. For intermediate values of k^2 (figure 9*b*) the curves seem to start off in the $1/(1-\tau^2)$ regime for small angles ($\phi < 40°$ say), but move into the large-k^2 regime for larger angles.

Figure 9(*c*) is in keeping with the results of Packham & Williams (1968). Their figure 1 is redrawn in figure 10 on reversed axes to the conform with figure 9(*c*). Energy-flux

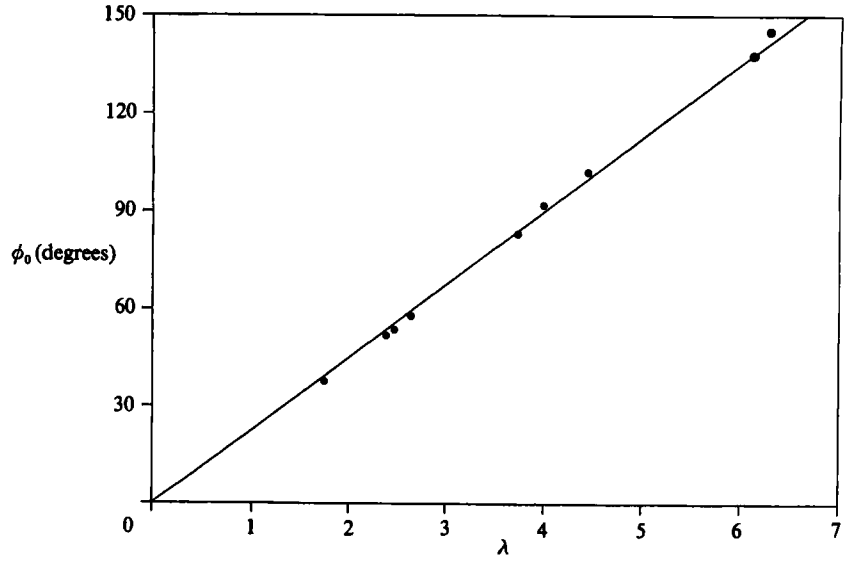

FIGURE 11. Angle of first zero reflection ϕ_0 against the incident wavelength λ: $r_0 = 0.5$. Line is the best straight-line fit to the points.

ratios were computed and plotted from their amplitude ratios. They investigated the propagation of a Kelvin wave around a wedge of variable angle. In their case no reflected Kelvin wave was possible. Energy that was not transmitted as an ongoing Kelvin wave was radiated as cylindrical Poincaré waves (see figure 10). These Poincaré waves could propagate because the frequency was super-inertial, and there was no channel.

They also found angles at which there was complete transmission, and that larger values of τ gave lower values for $R\%$. Their problem gives no meaning to k^2, since there is no natural lengthscale with which to non-dimensionalize the incident wavelength. However, large k^2 (as in figure 9*c*) in the bend in a channel would be expected to correspond most closely to their problem, since then the Poincaré modes are almost propagating, and they do have propagating Poincaré modes.

Figure 11 shows a plot of the first angle of complete transmission, ϕ_0, against the incident wavelength λ. The figure includes results from various values of k^2 and τ. A linear relationship was found. Thus the width of the 'lobes' in the $R\%$ *vs.* ϕ plots is directly proportional to the incident wavelength. This result is also found in diffraction theory in other fields.

This relationship between the width of the lobes and the incident wavelength λ is consistent with the linear relationship between $R\%$ and λ^{-2} for large λ and fixed ϕ found earlier. The relationship between $R\%$ and ϕ is almost quadratic for small ϕ (i.e. $R\% \propto \phi^2$, see, for example, figure 9*a*), so for a fixed ϕ, $R\%$ would be proportional to λ^{-2}.

6.5. $\tau = 0.803$, *various* k^2, *various* r_0, *variable* ϕ

So far all the results for the annular bend have been for a fixed inside radius, $r_0 = 0.5$. Figure 12 shows the effect of varying this 'sharpness' for medium and large values of k^2. In both cases, increasing the sharpness (decreasing r_0) gives rise to higher reflection coefficients. Not only are the peak values of the lobes increased, but the

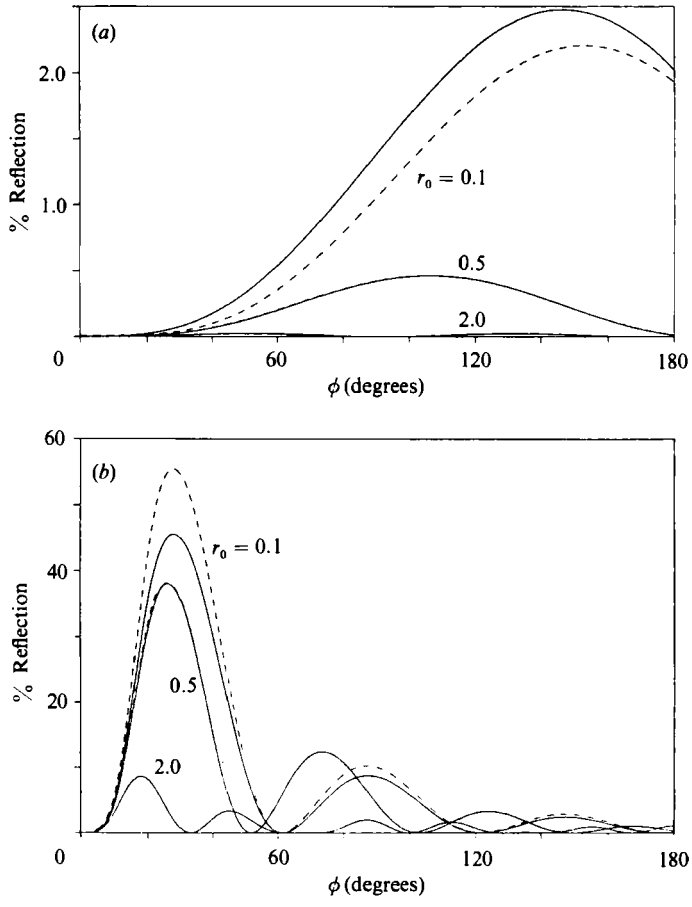

FIGURE 12. Reflection coefficient against bend angle ϕ for various values of the inside radius r_0: $\tau = 0.803$. Solid lines are $R\%$, dashed lines are $100-T\%$. (*a*) $k^2 = 0.2$; (*b*) 2.467.

constant of proportionality between the width of the lobe ϕ_0 and the incident wavelength is increased.

For very sharp bends ($r_0 = 0.1$) there is a significant discrepancy between $R\%$ and $100-T\%$, and the velocities fail to match precisely. Also there are large velocities in the region of the inside bend, especially for small k^2. These problems are exactly the same as were encountered when this method was applied to a so-called 'rectangular bend'. This bend was right-angled with a rectangle comprising region 2 instead of a sector of an annulus. Thus there was a discontinuity in the direction of the boundary by 90° at two points. Pneuli & Pekeris (1968) showed that near a corner of angular opening π/μ ($\mu < 1$), the solution is singular, giving rise to velocities which are $O(r^{\mu-1})$. Thus, at the inside corner of the rectangular bend, where $\mu = \frac{2}{3}$, a singularity will occur.

Hence it is not surprising that the method of expressing the solution as a harmonic basis functions failed in the rectangular bend, since such a series is incapable of representing the singularity. Nor is it surprising that the method breaks down in the annular bend as $r_0 \to 0$, and that large velocities are observed near the inside corner.

However, the rectangular bend gave qualitatively similar results to the annular bend in terms of reflection coefficients. The shape of figures 2 and 5 could be

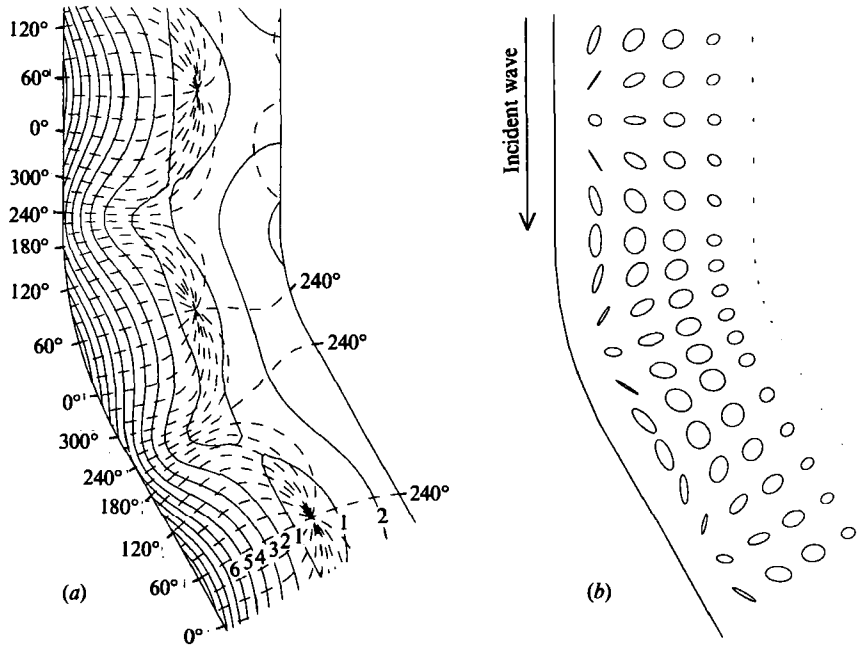

FIGURE 13. Same as figure 7 except $r_0 = 2.0$. Derived values: $R\% = 0.733\%$, $100 - T\% = 0.738\%$.

reproduced, although the magnitudes of the reflection coefficients were much higher because of the increased sharpness.

Figure 13 shows the solution in a bend of 30° with a large inside radius.The parameters are the same as in figure 7, except that the inside radius has been increased from 0.5 to 2.0, causing the reflection coefficient to drop from 36 to 0.7 %. The solution is no longer dominated by Poincaré modes. It is quite remarkable that bends to the left and bends to the right of the same angle (e.g. figures 7 and 8) have similar solutions and identical reflection coefficients, whereas changing the inside radius and leaving the angle alone (e.g. figure 13) has a major impact upon the solution and reflection coefficient.

7. Conclusions

The bend acts as a 'diffraction grating'. For certain bend angles there is total transmission, and between these angles there are 'lobes' of high reflection. These lobes form a diffraction pattern that spreads out as the incident wavelength increases. The width of the lobes is proportional to the wavelength, as in other types of waves in optics, electromagnetism, etc. The constant of proportionality depends on the inside radius of the bend.

It was found that bends to the left give rise to the same reflection coefficient as bends to the right of the same angle, irrespective of the degree to which the incident Kelvin wave is trapped against one wall (as measured by the Rossby radius).

For bends of fixed angle the reflection coefficient for large wavelengths was found to be proportional to the square of the ratio of the channel width to the incident wavelength. The constant of proportionality increases as the inside radius of the bend decreases.

Just below the critical frequency at which Poincaré-mode propagation becomes possible, this mode starts to dominate the solution, although while this mode is still evanescent it cannot contribute to the energy-flux budget. This result is consistent with Brown's (1973) result just above the critical frequency in a closed channel.

The method of solution breaks down for sub-inertial frequency waves, for unknown reasons. The method also breaks down as the inside radius of the bend tends to zero, because there is a singularity in the velocity field near corners whose angular opening is greater than 180°, as shown by Pneuli & Pekeris (1968). To correctly solve the problem in a geometry which has such a corner, the form of the solution must be capable of expressing a singularity.

The reflection coefficient of the internal tide in Knight Inlet at a 90° bend was found to be very small, $< 0.1\,\%$. Data from Knight Inlet are compatible with this result, in the sense that the vertical profiles of amplitude and phase of the M_2 constituent of velocity and density oscillations can be represented as a superposition of up-inlet-propagating vertical modes only, without having to include reflected modes. However, an accurate determination of the reflection coefficient for each vertical mode was not possible. The new data show that the internal tide in Knight Inlet cannot be represented by only one internal mode, as Freeland (1984) was forced to assume because he had current meters at only two depths. Further details are available in Webb (1985) and Webb & Pond (1986). Note that the results of this paper are equally applicable to a bend in any channel, and to barotropic tides.

This research was supported by the Natural Sciences and Engineering Research Council of Canada Grant A-8301. Personal support for A. J. Webb was also received from the Canadian Commonwealth Scholarship and Fellowship Plan. The authors wish to thank H. J. Freeland and D. M. Farmer for originally suggesting the problem.

REFERENCES

BLACKFORD, B. L. 1984 Effect of a tidal stream on internal wave observations and prediction. *Atmosphere–Ocean Phys.* **22**, 125–143.

BROWN, P. J. 1973 Kelvin wave reflection in semi-infinite canal. *J. Mar. Res.* **31**, 1–10.

BUCHWALD, V. T. 1968 The diffraction of Kelvin waves at a corner. *J. Fluid Mech.* **31**, 193–205.

FREELAND, H. J. 1984 The partition of internal tidal motions in Knight Inlet, British Columbia. *Atmosphere–Ocean Phys.* **22**, 144–150.

HENDERSHOTT, M. C. & SPERANZA, A. 1971 Co-oscillating tides in long, narrow bays; the Taylor problem revisited. *Deep-Sea Res.* **18**, 959–980.

LEBLOND, P. H. & MYSAK, L. A. 1978 *Waves in the Ocean.* Elsevier.

PACKHAM, B. A. & WILLIAMS, W. E. 1968 Diffraction of Kelvin waves at a sharp bend. *J. Fluid Mech.* **34**, 517–529.

PNEULI, A. & PEKERIS, C. L. 1968 Free tidal oscillations in rotating flat basins of the form of rectangles and of sectors of circles. *Phil. Trans. R. Soc. Lond.* A**263**, 149–171.

TAYLOR, G. I. 1920 Tidal oscillations in gulfs and rectangular basins. *Proc. Lond. Math. Soc.* **20**, 148–181.

WEBB, A. J. 1985 The propagation of the internal tide around a bend in Knight Inlet, B.C. Ph.D. thesis, University of British Columbia.

WEBB, A. J. & POND, S. 1986 A modal decomposition of the internal tide in a deep, strongly stratified inlet–Knight Inlet, B.C. *J. Geophys. Res.* (in press).